Hydrogen Bond Networks of Dimethylsulfoxide (DMSO) Pentamer

Alhadji Malloum[†,◇,*] and Jeanet Conradie[†,‡]

[†] Department of Chemistry, University of the Free State, PO BOX 339, Bloemfontein 9300, South Africa.

[◇] Department of Physics, Faculty of Science, University of Maroua, PO BOX 46, Maroua, Cameroon.

[‡]Department of Chemistry, UiT - The Arctic University of Norway, N-9037 Tromsø, Norway.

October 6, 2022

ABSTRACT: Understanding of clusters of dimethylsulfoxide (DMSO) is important in several applications in Chemistry. Despite its importance, very few studies of DMSO clusters, $(DMSO)_n$, have been reported in comparison to systems such as water clusters or methanol clusters. In order to provide further understanding of DMSO clusters, we investigated the structures and non-covalent interactions of the $(DMSO)_n$, $n = 5$. Therefore, the potential energy surface (PES) of the DMSO pentamer has been examined using classical molecular dynamics. The structures generated using classical molecular dynamics are further optimized at the PW6B95D3/aug-cc-pVDZ level of theory. To comprehend the non-covalent bondings in the DMSO pentamer, we carried out a quatum theory of atoms in molecule (QTAIM) analysis. In addition, the effects of temperature on the structural stability is investigated between 20 and 500 K. It comes out that seven different kind of non-covalent bondings can be found in DMSO pentamers.

KEYWORDS: DMSO pentamer; Non-Covalent Bondings; Structures; Relative energies; QTAIM analysis.

1 Introduction

Dimethylsulfoxide (DMSO) is a solvent that is often used in industries and in Chemistry. Understanding its behaviour and processes taking place therein at molecular level are thus very important. Structures of DMSO clusters are important for the description of liquid DMSO. By using the quantum cluster equilibrium (QCE) theory [1–5], one can determine and compute some interesting properties of liquid DMSO provided the structures of DMSO clusters are known. QCE uses the Cartesian coordinates, the relative energies, as well as the harmonic or anharmonic frequencies of DMSO clusters to determine the properties of liquid DMSO. In addition, DMSO clusters are very useful for theoretical description of processes taking place in DMSO solution. DMSO clusters can be used for example in the description of solvation processes of ions in DMSO, or ion transfer processes from/to DMSO. Despite its importance, very few studies of DMSO clusters, $(DMSO)_n$, have been reported in comparison to systems such as water clusters [6–10] or methanol clusters [11–14].

Venkataramanan *et al.* [15] investigated the structures of the DMSO clusters from dimer to 13-mer using different computational levels of theory. Their investigations have been limited to some structures where linear arrangements of DMSO molecules in the clusters were found more favorable. Therefore, the structures reported by the authors are not necessarily the most favorable structures on the potential energy surfaces (PESs) of the considered clusters. For these linear structures of the DMSO clusters, the authors reported the binding energies using M05-2X, M06-2X, B3LYP, and MP2 levels of theory. In addition, Venkataramanan and Suvitha [16] reported the nature of bonding and cooperativity for the structures of DMSO clusters from dimer to octamer, $(DMSO)_{n=2-8}$. The authors have carried out the calculations using the B3LYP-D3 functional associated to the 6-311++G(d,p) basis set. The authors showed that the computed binding energies and polarizabilities are evidence of the existence of cooperativity effect in linear DMSO clusters. It is worth noting that Venkataramanan and Suvitha [15] have also considered linear arrangements of the DMSO molecules in the studied clusters. Recently, we thoroughly investigated the PES of the DMSO clusters from dimer to tetramer at the MP2/aug-cc-pVDZ level of theory [17]. In addition, we reported the study of non-covalent bondings and the binding energies using 10 different DFT functionals. The functionals are benchmarked to the DLPNO-CCSD(T)/CBS level of theory. The study showed that the functionals PW6B95D3 and ωB97XD are the most suitable functionals for the study of the DMSO clusters [17]. Therefore, in the current investigation, we adopt the PW6B95D3 functional to study the DMSO pentamer. Apart from the two aforementioned studies [15,16], to the best of our knowledge, no explicit investigations of DMSO clusters have been reported in the literature. However, some investigations based on the interactions of DMSO with other molecules have been reported by few authors. Nikolakis and coworkers [18] reported the investigation of the DMSO-fructose and DMSO-water binary mixture using classical molecular dynamics and *ab-initio* methods. Zakharov *et al.* [19] reported the interactions of water-DMSO mixtures with cellulose. Besides, several authors reported the investigation of DMSO-water binary mixture using different computational approaches [20–22].

It follows from the exploration of the literature, that very few studies have been devoted to DMSO clusters. Although DMSO clusters from dimer to 13-mer have been reported, only linear structures (linear arrangements of molecules in clusters) have been identified as most favorable. Consequently, no explicit exploration of the potential energy surface of the clusters has been reported. Considering the role of all possible isomers in the accurate description of the cluster's population, it is important to

* *E-mail: MalloumA@ufs.ac.za; Tel: +237 695 15 10 56*

investigate all possible structures of a specific DMSO $n-$mer. Therefore, in this work, we performed a thorough exploration of the potential energy surface of the DMSO pentamer using two incremental levels of theory. Initial configurations are generated using classical molecular dynamics. The generated configurations are further optimized at the PW6B95D3/aug-cc-pVDZ level of theory. Furthermore, the effects of temperature on the structural stability are assessed between 20 and 500 K. Finally, we carried out a QTAIM analysis of the five lowest energy isomers to find all possible non-covalent bondings in the DMSO pentamer.

2 Methodology

In this section, we are presenting the theoretical and computational details of the investigations performed in this work. We start by presenting the method used for the sampling of initial guessed structures (see subsection 2.1). Finally, we present some specific details on the computational methods and the programs used for the investigations (see subsection 2.2).

2.1 Sampling initial structures

The most important task in the exploration of a potential energy surface (PES) is the sampling of the possible geometries (or structures). In this work, we used classical molecular dynamics as implemented in ABCluster[23,24] for the geometry sampling. The ABCluster has been used to generate several initial geometries of the DMSO pentamer for higher order optimization. To generate the geometries, ABCluster uses a classical potential which consider only electrostatic and Lenard-Jones contributions. It is expressed by the following equation:

$$U=\sum_{I=1}^{N}\sum_{J<I}^{N}\sum_{i_I}\sum_{j_J}\left(\frac{e^2}{4\pi\varepsilon_0}\frac{q_{i_I}q_{j_J}}{r_{i_Ij_J}}+4\varepsilon_{i_Ij_J}\left(\left(\frac{\sigma_{i_Ij_J}}{r_{i_Ij_J}}\right)^{12}-\left(\frac{\sigma_{i_Ij_J}}{r_{i_Ij_J}}\right)^{6}\right)\right). \quad (1)$$

Where I and J are the indices of the molecules, i_I and j_J are the indices of the atoms in molecules I and J, respectively. $r_{i_Ij_J}$ is the distance between atom i_I and j_J. There are three parameters to set in order to achieve the desired accuracy for exploration of PESs using ABCluster: the maximum cycle number g_{max}, the size of the trial solution population SN, and the scout limit g_{limit}. In this work, we used $g_{max}=5000$, $SN=60$, and $g_{limit}=4$. ABCluster generates several structures that are similar one to another. Therefore, from the generated structures, we select those that are different one from another for further optimization at the PW6B95D3/aug-cc-pVDZ level of theory. ABCluster has been used in our previous works to generate geometries of ammonia clusters[25–27], water clusters[28], and ethanol clusters[29,30]. Furthermore, ABCluster has been used in atmospheric and environmental sciences in order to locate the most stable structures of atmospheric clusters[31–34]. Recently, a compilation of several studies, which have successfully used ABCluster for different applications, has been reported by Zhang and Glezakou[35]. Therefore, we are very confident that the geometries generated by ABCluster are reliable and can be used for higher order optimization.

2.2 Computational details

Initial guessed structures generated by ABCluster are optimized at the PW6B95D3/aug-cc-pVDZ level of theory. The PW6B95D3 functional[36] has been used in our previous works and has been found to be among the best functional in calculating the binding energies of ethanol clusters[37] and ammonia clusters[38]. In addition, PW6B95D3 has shown a good performance in computing the interaction energies of acetonitrile clusters[39]. Gaussian 16 suite of programs[40] is used to optimize the geometries from ABCluster. Frequencies are calculated at the same computational level in Gaussian 16. The optimization have been performed using the *tight* option of the optimization to get more reliable global and local minima. The *ultrafine* grid is used for accurate integrals calculations.

Temperature effects are assessed between 20 to 500 K (temperature near the boiling point of DMSO liquid) using canonical distribution. It is well known that the structural stability depends on the temperature[6,7,41–43]. The probabilities are calculated using the Boltzmann distribution:

$$\mathscr{P}_k(T)=\frac{\exp\left(-\beta G_k(T)\right)}{\sum_i \exp\left(-\beta G_i(T)\right)}. \quad (2)$$

Where, $\beta=k_BT$, k_B is the Boltzmann constant, $G_k(T)$ is the free energy of the kth isomer of the DMSO pentamer at temperature T. The probabilities are calculated using the program **TEMPO** published by Fifen *et al.*[44,45]. We have used TEMPO is our past works to assess the effects temperature[46–50].

To comprehend the nature of non-covalent bondings (and therefore, the hydrogen bond Networks) of the DMSO pentamer, we carried out a QTAIM analysis of the five most stable structures. The AIMAll program[51] is used for QTAIM analysis.

3 Results and discussions

We start by presenting the located structures of the DMSO pentamer and their relative energies as optimized at the PW6B95D3/aug-cc-PVDZ level of theory (see subsection 3.1). Then we present the effects of temperature on the located structures by reporting their relative probabilities as function of temperature (see subsection 3.1). Finally, we present the QTAIM analysis and the non-covalent bondings available in the structures of the DMSO pentamer (see subsection 3.2).

3.1 Structures and relative population of DMSO pentamer

We have optimized with the PW6B95D3 functional all the structures generated using ABCluster. After full optimization of the structures, few geometries ended to be the same isomers. We have then eliminate all redundant geometries to select 37 isomers of the DMSO pentamer. In Figure 1 and Figure 2, we report the selected isomers of the DMSO pentamer. These figures include also the relative energies of the isomers with ZPE corrections. The reported isomers cover the relative energy spectrum from 0.0 to 14.5 kcal/mol.

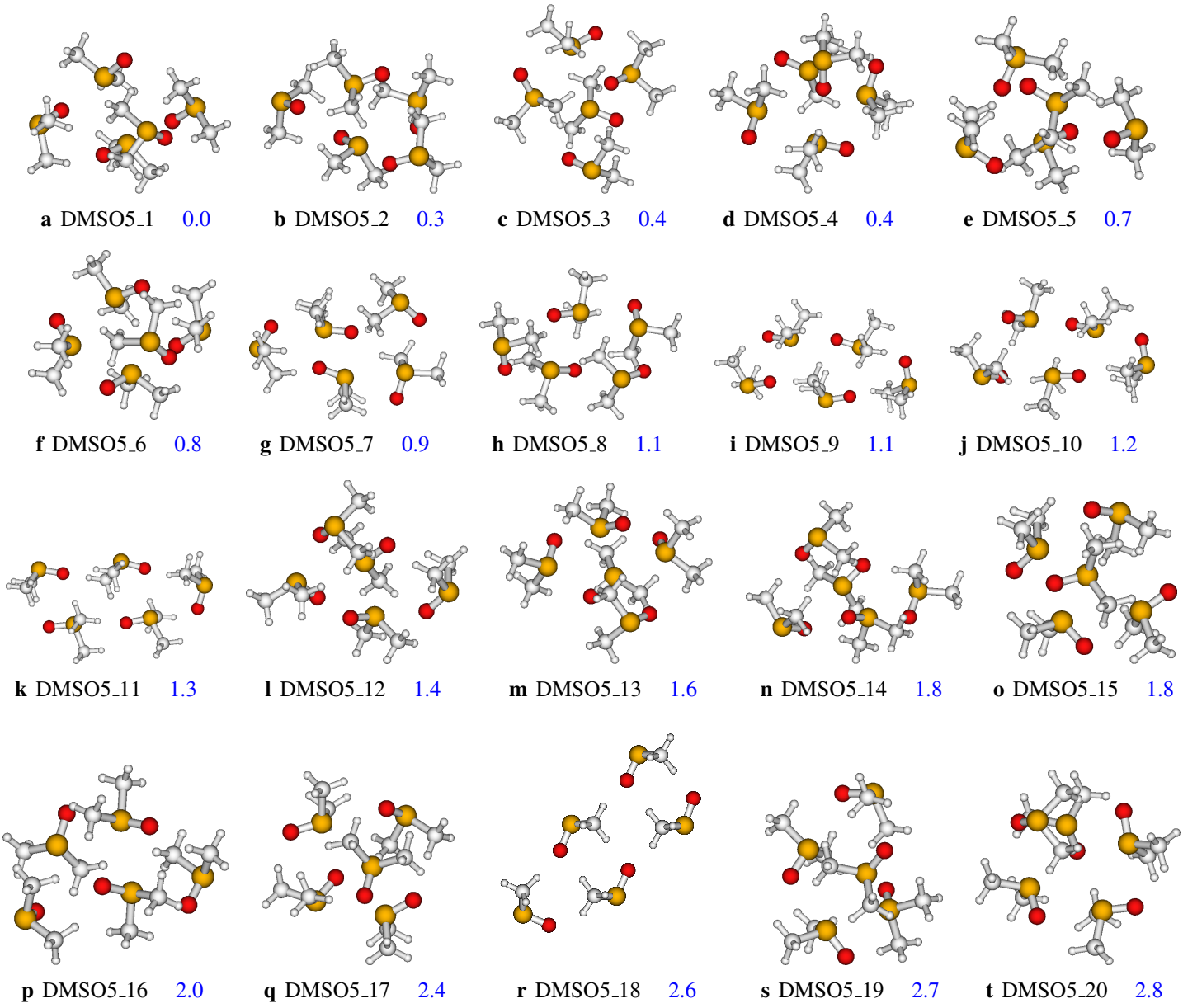

Fig. 1 Structures and relative energies of DMSO pentamer at the PW6B95D3/aug-cc-pVDZ level of theory. Energies (in kcal/mol) include zero point energy (ZPE) corrections. Small gray spheres are hydrogen atoms, big gray spheres are carbon atoms, yellow spheres are sulfur atoms while red spheres are oxygen atoms. The ZPE corrected electronic energy of **DMSO5_1** is −2768.281 478 au.

As can be seen in Figure 1 and Figure 2, the structures are reported in the increasing order of their relative stability. The most stable structure is the **DMSO5_1** isomer. **DMSO5_1** is formed of a cyclic trimer and a dimer branched in folded position. The next three stable isomers (**DMSO5_2**, **DMSO5_3**, and **DMSO5_4**) lay at 0.3, 0.4 and 0.4 kcal/mol above **DMSO5_1**, respectively. These three isomers are constituted of a folded cyclic tetramer and one DMSO molecule interacting with it. Generally, the located isomers of the DMSO pentamer have no definite symmetry, and exhibit an amorphous behaviour. Nevertheless, some structural trends can be seen in some isomers. Several isomers can be seen as folded cyclic structure of the DMSO pentamer (see for example isomers **DMSO5_7** to **DMSO5_11** in Figure 1). Some isomers of the DMSO pentamer can be seen as folded cyclic tetramer and one DMSO molecule in branched position (see for example isomers **DMSO5_31** to **DMSO5_35** in Figure 2). Furthermore, one should note that some isomers of the DMSO pentamer does not fit into the description of cyclic and branched cyclic structure, and thus will be considered amorphous.

It comes out from the literature that very few authors reported the structures of the DMSO clusters. The only meaningful study of the DMSO clusters were performed by Venkataramanan and coworkers [15,16]. The authors reported the structures of the DMSO clusters for $n = 2 - 13$. The optimization of the structures have

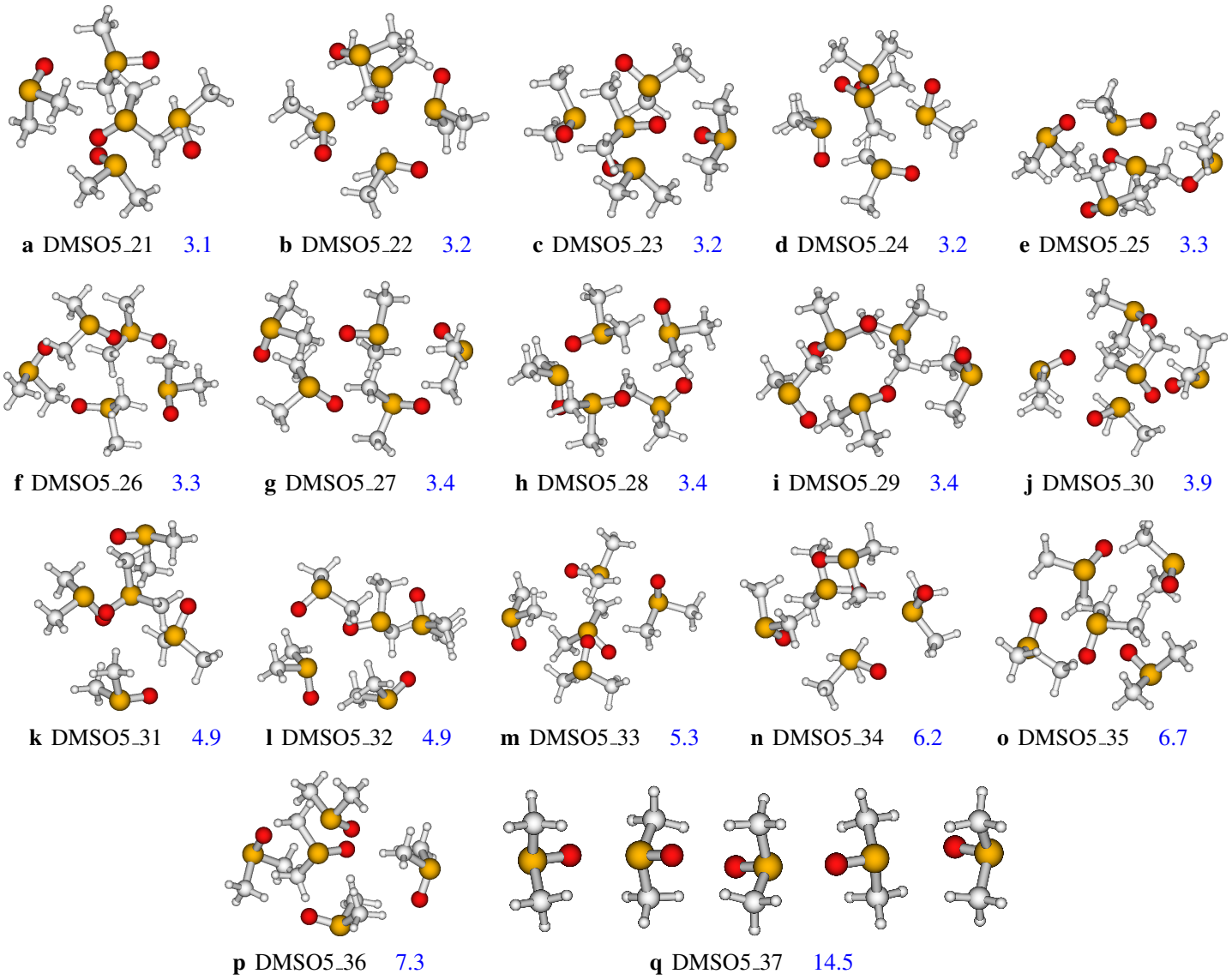

Fig. 2 Figure 1 continue - Structures and relative energies of the DMSO pentamer at the PW6B95D3/aug-cc-pVDZ level of theory. Energies (in kcal/mol) include zero point energy (ZPE) corrections. Small gray spheres are hydrogen atoms, big gray spheres are carbon atoms, yellow spheres are sulfur atoms while red spheres are oxygen atoms.

been performed using three DFT functionals. Their investigations showed that only linear arrangement of DMSO molecules in the clusters are favorable. Thus, for the DMSO pentamer, the authors reported two different linear structures labelled **DMSO5_18** and **DMSO5_37** in Figure 1 and Figure 2. The isomer **DMSO5_18** is constituted of two dimers and the DMSO monomer interacting together in linear arrangement. The isomer **DMSO5_18** which has been claimed to be the most favorable, is reported in this work to be 2.6 kcal/mol higher in energy. The isomer **DMSO5_37** is the least stable among the structures of the DMSO pentamer located in this work. Moreover, its relative energy exhibit a considerable gap as compared to other isomers, indicating its less stability. This can be understandable, considering the fact that folded structures can form more non-covalent interactions as compared to linear structures. Moreover, it has been found in our previous studies on methanol clusters and ethanol clusters, that the linear structures are less stable than folded cyclic structures and branched cyclic structures [14,37].

In addition to the relative energies at the PW6B95D3/aug-cc-pVDZ level of theory, we optimized all 37 isomers of the DMSO pentamer at the ωB97XD/aug-cc-pVDZ and the M06/aug-cc-pVDZ levels of theory. We reported the relative energies at these levels of theory in the related data article. The relative energies at these three levels of theory follow different trends. The three levels of theory predicted different isomers to be the most stable structure of the DMSO pentamer. At the ωB97XD/aug-cc-pVDZ level of theory, the isomer **DMSO5_12** is predicted to be the most stable isomer, while the isomer **DMSO5_16** is found to be the

most stable structure at the M06/aug-cc-pVDZ level of theory. However, it has been found that the three levels of theory predicted the linear isomer **DMSO5_37** to be the least stable structure. One should note that up to 09 isomers reported in Figure 1 and Figure 2 have optimized to a transition state structures at the M06/aug-cc-pVDZ level of theory. Moreover, the relative energies at the M06/aug-cc-pVDZ level of theory are unusually high as compared to those calculated at PW6B95D3/aug-cc-pVDZ and ωB97XD/aug-cc-pVDZ levels of theory.

Having located 35 different isomers of the DMSO pentamer, we are now interested in understanding their contributions to the cluster's population. Thus, we calculated the temperature-dependent probabilities of the isomers of the DMSO pentamer between 20 and 500 K. The calculated probabilities are plotted in Figure 3. Most of the isomers have no contributions to the clusters' population with a probability of 0% for the investigated temperature range. Some isomers have their probabilities lower than 5% at high temperatures. In this work, we consider all contributions lower than 5% to be negligible. Consequently, to avoid cumbersomeness, we present in Figure 3 only the structures having a probability equal to or higher than 5%.

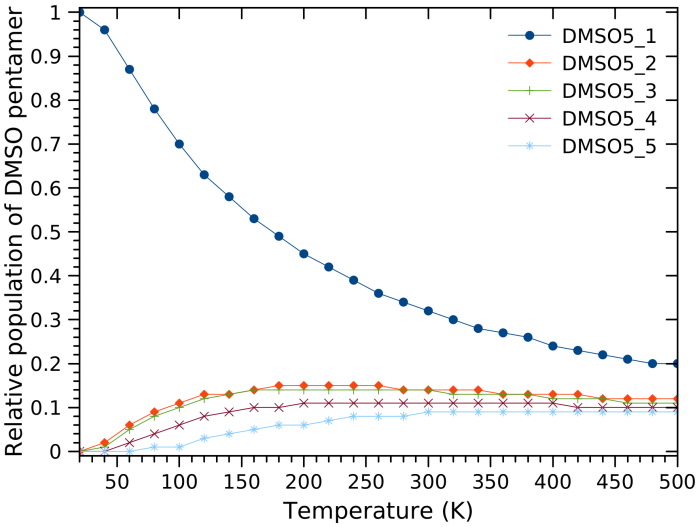

Fig. 3 Relative population/probabilities of the structures of the DMSO pentamer between 20 and 500 K. We reported in this plot only the structures with probabilities higher or equal 5%.

The results show that only five isomers (the first five most stable isomers in Figure 1) have meaningful contributions to the cluster's population. All other isomers have negligible contributions to the population of the DMSO pentamer, according to the Boltzmann distribution. The isomer **DMSO5_1** dominates the cluster's population between 20 and 500 K. At low temperatures, the compactness of **DMSO5_1** is responsible of its high stability, hence its 100% dominance. With increasing temperature, the isomer **DMSO5_1** loses its compactness, therefore, its probability decreases. However, **DMSO5_1** has higher stability than the other isomers at all temperatures (20 to 500 K). This result indicates that with the increase of temperature the isomer **DMSO5_1** still has the lowest total Gibbs free energy. It also indicates the strong stability of the isomer **DMSO5_1**. The other four isomers (**DMSO5_2** to **DMSO5_5**) contribute to the cluster's population with about 10% each, for temperatures higher than 100 K (see Figure 3). Thus, it can be concluded that the population of the DMSO pentamer is constituted of the contribution from the isomers **DMSO5_1** to **DMSO5_5**. This result shows that only the five most stable isomers of the DMSO pentamer are required to compute the gas phase properties of the DMSO pentamer between 20 and 500 K, and the stability order stayed the same. As we stated in the methodology section, several authors reported the change of the stability order of the isomer when the temperature is increased. Detailed investigations have been reported for the water clusters[6,7,41–43]. In addition, we have also reported the effects of temperature on the structural stability of the protonated ammonia clusters[52,53], and the results were supported by experimental data.

3.2 Non-covalent interactions in DMSO pentamer

Knowledge of non-covalent bonding is important to properly study the bonding networks in DMSO clusters. To comprehend and identify the interactions taking place in DMSO clusters, we carried out a QTAIM analysis for the five low energy isomers of the DMSO pentamer. QTAIM analysis explore the electron density, ρ, hypersurface of molecules to identify all the extrema (minima, maxima and saddle points). The extrema, where the first order derivatives of the electron density vanishes, are also called critical points. The nature of the critical points is defined by the signature of the second derivatives of the electron density, $\nabla^2\rho$: atom critical point (3, -3); bond critical point (3, -1); ring critical point (3, 1); and cage critical point (3, 3). Two atomic points are usually linked by a bond path. Each bond path has a bond critical point (BCP), which is located where the electron density passes through its minimum on the path. The study of the topology of ρ, $\nabla^2\rho$, and the properties of BCP provides a universal description of chemical bondings between atoms[54]. It is possible to identify the type of a given chemical bonding by knowing the value of the electron density, and the Laplacian of the electron density, at a bond critical point[55]. When the Laplacian of ρ at a BCP is negative, the corresponding bonding is a covalent bond. However, when the Laplacian of ρ at a BCP is positive, the corresponding bonding is a non-covalent bonding[56,57]. Weak hydrogen bondings as well as van der Waals interactions are attributed to bondings where the Laplacian of ρ is positive, and ρ is weak at the corresponding BCPs[55]. To attribute the label **hygrogen bonding** to a chemical bonding, the value of ρ and $\nabla^2\rho$ at BCP should be between 0.024 and 0.139 ea_0^{-5} for $\nabla^2\rho$, and 0.002 and 0.035 ea_0^{-3} for ρ[58]. After performing the QTAIM analysis for the five lowest energy structures of the DMSO pentamer, we reported in Figure 4 the bond paths and the critical points. Solid lines are used to represent covalent bondings, while dashes lines are used to represent non-covalent bondings. In addition, the properties of BCPs are reported in the related data article. These properties include the electron density, the Laplacian of the electron density, the ellipticity, and more.

It follows from our investigations that there are seven different

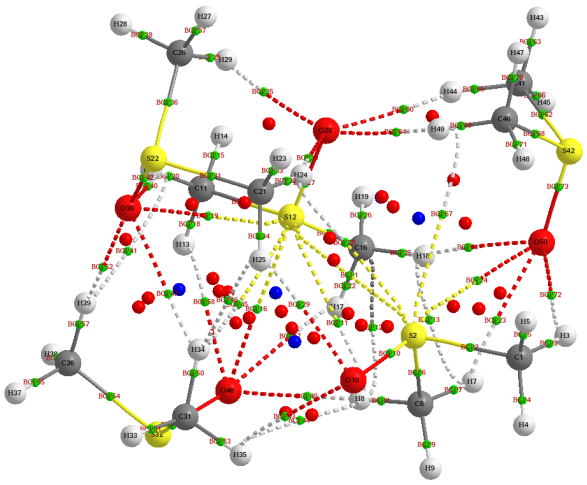

a DMSO5_1 0.0

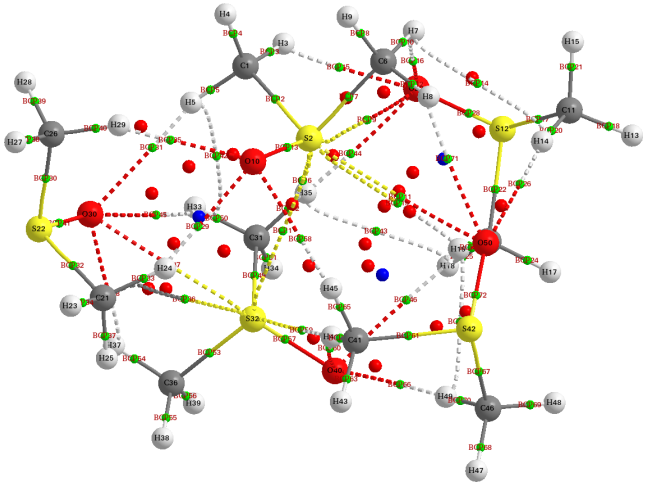

b DMSO5_2 0.3

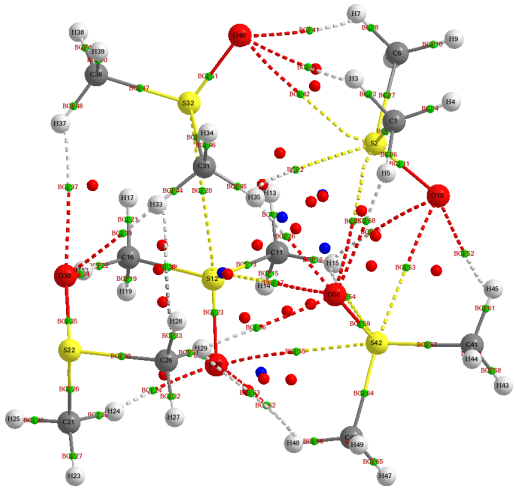

c DMSO5_3 0.4

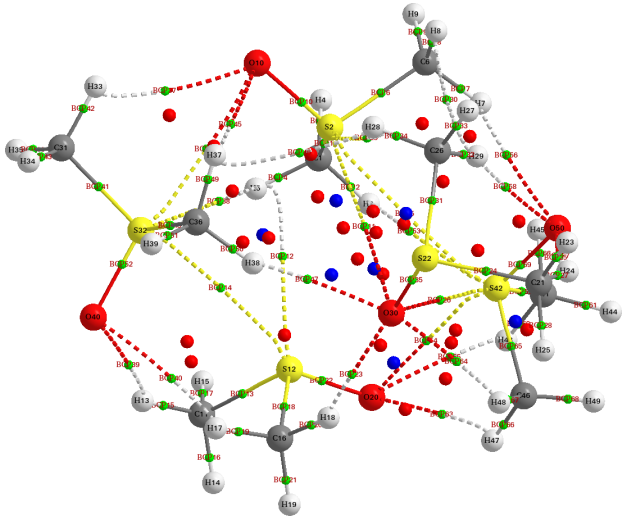

d DMSO5_4 0.4

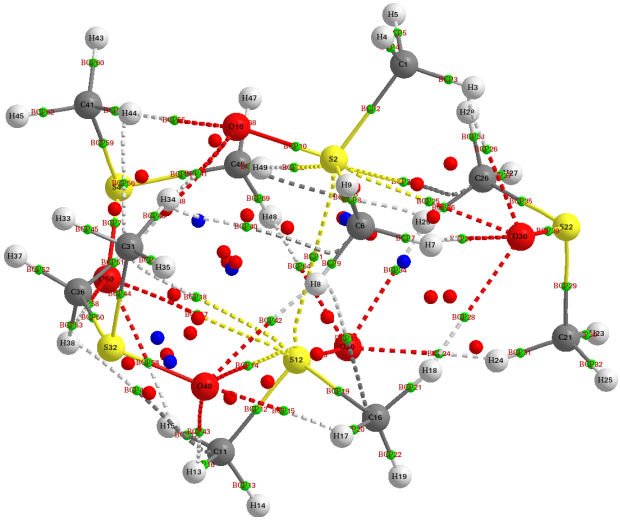

e DMSO5_5 0.7

Fig. 4 Bond critical points (BCPs), ring critical points (RCPs), cage critical points (CCPs) and bond paths (BPs) of the five most stable structures of the DMSO pentamer. Covalent bond paths are reported in solid lines while dash lines represent non-covalent bond paths.

Table 1 Maximum and Minimum values of the electron density, ρ, and the Laplacian of the electron density, $\nabla^2\rho$, at bond critical points.

	ρ (ea_0^{-3})		$\nabla^2\rho$ (ea_0^{-5})	
Bonding	Min	Max	Min	Max
CH···O	0.0069	0.0167	0.0257	0.0487
CH···S	0.0035	0.0084	0.0103	0.0309
CH···C	0.0038	0.0054	0.0144	0.0220
S···O	0.0026	0.0132	0.0076	0.0406
S···C	0.0041	0.0048	0.0126	0.0153
S···S	0.0066	0.0097	0.0184	0.0282
H···H	0.0032	0.0051	0.0128	0.0200

types of non-covalent interactions in DMSO pentamers. These non covalent interactions as well as the maximum and minimum values of ρ and $\nabla^2\rho$ at the bond critical points are reported in Table 1. Although they are reported in Table 1, very few CH···C and S···C bondings are identified in DMSO pentamers. The most common non-covalent bonding is the CH···O hydrogen bonding. The results show that the hydrogen bondings are the strongest non-covalent bondings in DMSO pentamers. Besides, the H···H bonding is the weakest non-covalent bonding of the DMSO pentamer considering the weak electron density at the corresponding BCPs. To get more insights on the relation between the stability of the isomers and their non-covalent interactions, we reported in Table 2 the type of number of non-covalent bondings for the five most stable structures. As can be seen in Table 2 the CH···O hydrogen bonding is the most common non-covalent bondings in DMSO pentamers. In addition, it has been found that the stability of the isomers is highly related to the number of CH···O hydrogen bondings. The most stable structure, **DMSO5_1**, has the highest number of CH···O hydrogen bondings (see Table 2). Besides, only few CH···C, S···S, and S···C bonding interactions are found.

Table 2 Type and number of non-covalent interactions in each of the five most stable structures of the DMSO pentamer. **DS5_1**-**DS5_5** represent **DSM5_1**-**DMSO5_5**, respectively.

Bonding	**DS5_1**	**DS5_2**	**DS5_3**	**DS5_4**	**DS5_5**
CH···O	15	14	13	12	14
CH···S	04	03	02	03	02
CH···C	01	00	01	00	04
S···O	08	08	08	09	08
S···C	00	01	00	00	01
S···S	01	01	01	02	01
H···H	04	04	01	02	01

4 Conclusions

In this work, we examined thoroughly the potential energy surface (PES) of the DMSO pentamer based on two different levels of approximation. We started by exploring the PES using classical molecular dynamics to identify all guessed structures. Then, the guessed structures are optimized using the PW6B95D3 DFT functional associated to the aug-cc-pVDZ basis set. After full optimization, thirty seven different isomers of the DMSO pentamer are located within 14.5 kcal/mol. The results show that most of the isomers of the DMSO pentamer exhibit an amorphous behaviour. However, some isomers are found to be having folded cyclic and branched cyclic configurations. After reporting the isomers and their relative energies, we examined the effects of temperature on the structural stability. It follows that the lowest energy structure has the highest probability in the cluster's population between 20 and 500 K. Furthermore, the results show that only the five most stable isomers have meaningful contribution to the DMSO pentamer's population. The contribution of other isomers are found to be negligible (probabilities $< 5\%$).

To identify possible non-covalent bondings in DMSO clusters, we carried out a QTAIM analysis for the first five low energy structures of the DMSO pentamer. The investigations show that seven non-covalent bonding can be identified in the DMSO pentamer. Among the identified non-covalent bondings, the CH···O hydrogen bonds are found to be the strongest non-covalent interactions. In addition, the H···H bondings are found to be the weakest chemical bonding in the DMSO pentamer.

Conflicts of interest

There are no conflicts of interest to declare.

Acknowledgements

The authors are grateful to the Center for High Performance Computing (CHPC) in South Africa for granting them access to their clusters and computational resources. The Norwegian Supercomputing Program (UNINETT Sigma2, Grant No. NN9684K) is acknowledged for computer time. We would also like to thank the Central Research Fund of the University of the Free State.

Supplementary material

The material is presented as data in brief article related to the present paper. It contains the Cartesian coordinates of all 37 optimized structures of the DMSO pentamer, at the PW6B95D3/aug-cc-pVDZ level of theory, and the relative energies at ωB97XD/aug-cc-pVDZ and M06/aug-cc-pVDZ levels of theory. It also contains the weighted free energies and weighted enthalpies for temperatures ranging from 20 to 500 K. In addition, QTAIM analysis data of the five most stable structures of the DMSO pentamer are also provided.

References

1 R. Ludwig, F. Weinhold, T. Farrar, Quantum cluster equilibrium theory of liquids part i: Molecular clusters and thermodynamics of liquid ammonia, Ber. Bunsen. Phys. Chem. 102 (1998) 197–204.

2 R. Ludwig, F. Weinhold, T. Farrar, Quantum cluster equilibrium theory of liquids part ii: Temperature dependent chemical shifts, quadrupole coupling constants and vibrational frequencies in liquid ammonia, Ber. Bunsen. Phys. Chem. 102 (1998) 205–212.

3 G. Matisz, W. M. Fabian, A.-M. Kelterer, S. Kunsági-Máté, Weinhold's qce model–a modified parameter fit. model study of liquid methanol based on mp2 cluster geometries, J. Mol. Struct. 956 (2010) 103–109.

4 B. Kirchner, C. Spickermann, S. B. Lehmann, E. Perlt, J. Langner, M. von Domaros, P. Reuther, F. Uhlig, M. Kohagen, M. Brüssel, What can clusters tell us about the bulk?: Peacemaker: Extended quantum cluster equilibrium calculations, Comput. Phys. Commun. 182 (2011) 1428–1446.

5 M. von Domaros, E. Perlt, Anharmonic effects in the quantum cluster equilibrium method, J. Chem. Phys. 146 (2017) 124114.

6 C. Pérez, M. T. Muckle, D. P. Zaleski, N. A. Seifert, B. Temelso, G. C. Shields, Z. Kisiel, B. H. Pate, Structures of cage, prism, and book isomers of water hexamer from broadband rotational spectroscopy, Science 336 (2012) 897–901.

7 Y. Wang, V. Babin, J. M. Bowman, F. Paesani, The water hexamer: cage, prism, or both. full dimensional quantum simulations say both, J. Am. Chem. Soc. 134 (2012) 11116–11119.

8 N. Sahu, G. Singh, A. Nandi, S. R. Gadre, Toward an accurate and inexpensive estimation of ccsd (t)/cbs binding energies of large water clusters, J Phys. Chem. A 120 (2016) 5706–5714.

9 D. Yuan, Y. Li, Z. Ni, P. Pulay, W. Li, S. Li, Benchmark relative energies for large water clusters with the generalized energy-based fragmentation method, J Chem. theory Comput. 13 (2017) 2696–2704.

10 A. Malloum, J. J. Fifen, Z. Dhaouadi, S. G. N. Engo, J. Conradie, Structures, relative stabilities and binding energies of neutral water clusters,$(h_2o)_{2-30}$, New J. Chem. 43 (2019) 13020–13037.

11 J. David, D. Guerra, A. Restrepo, Structural characterization of the (methanol)4 potential energy surface, J. Phys. Chem. A 113 (2009) 10167–10173.

12 S. Kazachenko, S. Bulusu, A. J. Thakkar, Methanol clusters (ch3oh)n: Putative global minimum-energy structures from model potentials and dispersion-corrected density functional theory, J. Chem. Phys. 138 (2013) 224303.

13 P.-J. Hsu, K.-L. Ho, S.-H. Lin, J.-L. Kuo, Exploration of hydrogen bond networks and potential energy surfaces of methanol clusters using a two-stage clustering algorithm, Phys. Chem. Chem. Phys. 19 (2017) 544–556.

14 A. Malloum, J. J. Fifen, J. Conradie, Solvation energies of the proton in methanol revisited and temperature effects, Phys. Chem. Chem. Phys. 20 (2018) 29184–29206.

15 N. S. Venkataramanan, A. Suvitha, Y. Kawazoe, Density functional theory study on the dihydrogen bond cooperativity in the growth behavior of dimethyl sulfoxide clusters, J. Mol. Liq. 249 (2018) 454–462.

16 N. S. Venkataramanan, A. Suvitha, Nature of bonding and cooperativity in linear dmso clusters: a dft, aim and nci analysis, J. Mol. Graph. Model. 81 (2018) 50–59.

17 A. Malloum, J. Conradie, Non-covalent interactions in dimethylsulfoxide (dmso) clusters and dft benchmarking, J. Mol. Liq. 350 (2022) 118522.

18 V. Nikolakis, S. H. Mushrif, B. Herbert, K. S. Booksh, D. G. Vlachos, Fructose–water–dimethylsulfoxide interactions by vibrational spectroscopy and molecular dynamics simulations, J. Phys. Chem. B 116 (2012) 11274–11283.

19 A. Zakharov, M. Voronova, A. Prusov, O. Surov, M. Radugin, T. Lebedeva, Interaction of water-dmso mixtures with cellulose, Russ. J. Phys. Chem. 80 (2006) 1295–1299.

20 D. N. Shin, J. W. Wijnen, J. B. Engberts, A. Wakisaka, On the origin of microheterogeneity: Mass spectrometric studies of acetonitrile- water and dimethyl sulfoxide- water binary mixtures (part 2), J. Phys. Chem. B 106 (2002) 6014–6020.

21 M. Voronova, T. Lebedeva, M. Radugin, O. Surov, A. Prusov, A. Zakharov, Interactions of water–dmso mixtures with cellulose, J. Mol. Liq. 126 (2006) 124–129.

22 N. Zhang, W. Li, C. Chen, J. Zuo, Molecular dynamics simulation of aggregation in dimethyl sulfoxide–water binary mixture, Comput. Theor. Chem. 1017 (2013) 126–135.

23 J. Zhang, M. Dolg, Abcluster: the artificial bee colony algorithm for cluster global optimization, Phys. Chem. Chem. Phys. 17 (2015) 24173–24181.

24 J. Zhang, M. Dolg, Global optimization of clusters of rigid molecules using the artificial bee colony algorithm, Phys. Chem. Chem. Phys. 18 (2016) 3003–3010.

25 A. Malloum, J. J. Fifen, J. Conradie, Structures and spectroscopy of the ammonia eicosamer, $(nh_3)_{n=20}$, J. Chem. Phys. 149 (2018) 024304.

26 A. Malloum, J. J. Fifen, J. Conradie, Large-sized ammonia clusters and solvation energies of the proton in ammonia, J. Comput. Chem. 41 (2020) 21–30.

27 A. Malloum, J. Conradie, Solvent effects on the structures of the neutral ammonia clusters, Comput. Theor. Chem. 1191 (2020) 113042.

28 A. Malloum, J. Conradie, Structures of water clusters in the solvent phase and relative stability compared to gas phase, Polyhedron 193 (2021) 114856.

29 A. Malloum, J. J. Fifen, J. Conradie, Exploration of the potential energy surface of the ethanol hexamer, J. Chem. Phys. 150 (2019) 124308.

30 A. Malloum, J. J. Fifen, J. Conradie, Theoretical infrared spectrum of the ethanol hexamer, Int. J. Quantum Chem. 120 (2020) e26234.

31 H. Li, J. Zhong, H. Vehkamaki, T. Kurtén, W. Wang, M. Ge, S. Zhang, Z. Li, X. Zhang, J. S. Francisco, et al., Self-catalytic reaction of so3 and nh3 to produce sulfamic acid and its implication to atmospheric particle formation, J. Am. Chem. Soc. 140 (2018) 11020–11028.

32 H. Zhang, W. Wang, S. Pi, L. Liu, H. Li, Y. Chen, Y. Zhang, X. Zhang, Z. Li, Gas phase transformation from organic acid to organic sulfuric anhydride: Possibility and atmospheric

fate in the initial new particle formation, Chemosphere 212 (2018) 504–512.

33 X. Ma, Y. Sun, Z. Huang, Q. Zhang, W. Wang, A density functional theory study of the molecular interactions between a series of amides and sulfuric acid, Chemosphere 214 (2019) 781–790.

34 D. Li, D. Chen, F. Liu, W. Wang, Role of glycine on sulfuric acid-ammonia clusters formation: Transporter or participator, J. Environ. Sci. 89 (2020) 125–135.

35 J. Zhang, V.-A. Glezakou, Global optimization of chemical cluster structures: Methods, applications, and challenges, Int. J. Quantum Chem. 121 (7) (2021) e26553.

36 Y. Zhao, D. G. Truhlar, Design of density functionals that are broadly accurate for thermochemistry, thermochemical kinetics, and nonbonded interactions, J. Phys. Chem. A 109 (2005) 5656–5667.

37 A. Malloum, J. J. Fifen, J. Conradie, Exploration of the potential energy surfaces of small ethanol clusters, Phys. Chem. Chem. Phys. 22 (2020) 13201–13213.

38 A. Malloum, J. Conradie, Accurate binding energies of ammonia clusters and benchmarking of hybrid dft functionals, Comput. Theor. Chem. 1200 (2021) 113236.

39 A. Malloum, J. J. Fifen, J. Conradie, Binding energies and isomer distribution of neutral acetonitrile clusters, Int. J. Quantum Chem. 120 (2020) e26221.

40 M. J. Frisch, G. W. Trucks, H. B. Schlegel, G. E. Scuseria, M. A. Robb, J. R. Cheeseman, G. Scalmani, V. Barone, G. A. Petersson, H. Nakatsuji, X. Li, M. Caricato, A. V. Marenich, J. Bloino, B. G. Janesko, R. Gomperts, B. Mennucci, H. P. Hratchian, J. V. Ortiz, A. F. Izmaylov, J. L. Sonnenberg, D. Williams-Young, F. Ding, F. Lipparini, F. Egidi, J. Goings, B. Peng, A. Petrone, T. Henderson, D. Ranasinghe, V. G. Zakrzewski, J. Gao, N. Rega, G. Zheng, W. Liang, M. Hada, M. Ehara, K. Toyota, R. Fukuda, J. Hasegawa, M. Ishida, T. Nakajima, Y. Honda, O. Kitao, H. Nakai, T. Vreven, K. Throssell, J. A. Montgomery, Jr., J. E. Peralta, F. Ogliaro, M. J. Bearpark, J. J. Heyd, E. N. Brothers, K. N. Kudin, V. N. Staroverov, T. A. Keith, R. Kobayashi, J. Normand, K. Raghavachari, A. P. Rendell, J. C. Burant, S. S. Iyengar, J. Tomasi, M. Cossi, J. M. Millam, M. Klene, C. Adamo, R. Cammi, J. W. Ochterski, R. L. Martin, K. Morokuma, O. Farkas, J. B. Foresman, D. J. Fox, Gaussian˜16 Revision A.03, gaussian Inc. Wallingford CT (2016).

41 R. M. Shields, B. Temelso, K. A. Archer, T. E. Morrell, G. C. Shields, Accurate predictions of water cluster formation,$(h_2o)_{n=2-10}$, J. Phys. Chem. A 114 (2010) 11725–11737.

42 B. Temelso, K. A. Archer, G. C. Shields, Benchmark structures and binding energies of small water clusters with anharmonicity corrections, J. Phys. Chem. A 115 (2011) 12034–12046.

43 A. Rakshit, T. Yamaguchi, T. Asada, P. Bandyopadhyay, Understanding the structure and hydrogen bonding network of (h 2 o) 32 and (h 2 o) 33 : an improved monte carlo temperature basin paving (mctbp) method and quantum theory of atoms in molecules (qtaim) analysis, RSC Adv. 7 (2017) 18401–18417.

44 J. J. Fifen, M. Nsangou, Z. Dhaouadi, O. Motapon, N.-E. Jaidane, Structures of protonated methanol clusters and temperature effects, J. Chem. Phys. 138 (2013) 184301.

45 J. J. Fifen, N. Agmon, Structure and spectroscopy of hydrated sodium ions at different temperatures and the cluster stability rules, J. Chem. Theory Comput. 12 (2016) 1656–1673.

46 A. Hattab, Z. Dhaouadi, A. Malloum, J. J. Fifen, S. Lahmar, N. Russo, E. Sicilia, Structures, binding energies, temperature effects, infrared spectroscopy of $[mg(nh_3)_{n=1-10}]^+$ clusters from dft and mp2 investigations, J. Comput. Chem. 40 (2019) 1707–1717.

47 A. Hattab, Z. Dhaouadi, A. Malloum, J. J. Fifen, S. Lahmar, N. Russo, E. Sicilia, Structures, binding energies and temperature effects $[mg(nh_3)_{n=1-10}]^{2+}$ clusters, Theor. Chem. Acc. 138 (2019) 71.

48 O. Boukar, J. J. Fifen, A. Malloum, Z. Dhaouadi, H. Ghalila, J. Conradie, Structures of solvated ferrous ion clusters in ammonia and spin-crossover at various temperatures, New J. Chem. 43 (2019) 9902–9915.

49 T. E. Da-yang, J. J. Fifen, A. Malloum, S. Lahmar, M. Nsangou, J. Conradie, Structures of the solvated copper (ii) ion in ammonia at various temperatures, New J. Chem. 44 (2020) 3637–3653.

50 A. Malloum, J. Conradie, Global and local minima of protonated acetonitrile clusters, New J. Chem. 44 (2020) 17558–17569.

51 T. A. Keith, Tk gristmill software, Overland Park KS, USA 11 (2019) 16, (aim.tkgristmill.com).

52 A. Malloum, J. J. Fifen, Z. Dhaouadi, E. S. G. Nana, N.-D. Jaidane, Structures and spectroscopy of protonated ammonia clusters at different temperatures, Phys. Chem. Chem. Phys. 18 (2016) 26827–26843.

53 A. Malloum, J. J. Fifen, Z. Dhaouadi, E. S. G. Nana, N.-D. Jaidane, Structures and spectroscopy of medium size protonated ammonia clusters at different temperatures, $h^+(nh_3)_{10-16}$, J. Chem. Phys. 146 (2017) 044305.

54 R. F. Bader, A bond path: a universal indicator of bonded interactions, J. Phys. Chem. A 102 (1998) 7314–7323.

55 S. J. Grabowski, What is the covalency of hydrogen bonding?, Chem. Rev. 111 (2011) 2597–2625.

56 R. G. Bone, R. F. Bader, Identifying and analyzing intermolecular bonding interactions in van der waals molecules, J. Phys. Chem. 100 (1996) 10892–10911.

57 I. Alkorta, F. Blanco, J. Elguero, J. A. Dobado, S. M. Ferrer, I. Vidal, Carbon···carbon weak interactions, J. Phys. Chem. A 113 (2009) 8387–8393.

58 U. Koch, P. L. Popelier, Characterization of cho hydrogen bonds on the basis of the charge density, J. Phys. Chem. 99 (1995) 9747–9754.